Proceedings of the ASME 2018 37th International Conference on Ocean, Offshore and Arctic Engineering
OMAE2018
June 17-22, 2018, Madrid, Spain

OMAE2018-78738

HYDRO-ELASTIC ANALYSIS OF A FLOATING BRIDGE IN WAVES CONSIDERING THE EFFECT OFTHE HYDRODYNAMIC COUPLING AND THE SHORE SIDES

Shi Deng
Department of Marine Technology
Norwegian University of Science and Technology
7491 Trondheim Norway
Email: shi.deng@ntnu.no

Shixiao Fu*
State Key Laboratory of Ocean Engineering
Shanghai Jiao Tong University
Shanghai, 200030 China
Email: shixiao.fu@sjtu.edu.cn

Torgeir Moan
Centre for Autonomous Marine Operations and Systems, Department of Marine Technology
Norwegian University of Science and Technology
7491 Trondheim Norway
Email: torgeir.moan@ntnu.no

Wei Wei
State Key Laboratory of Ocean Engineering
Shanghai Jiao Tong University
Shanghai, 200030 China
Email: weiwei_allen@126.com

Zhen Gao
Centre for Autonomous Marine Operations and Systems, Department of Marine Technology
Norwegian University of Science and Technology
7491 Trondheim Norway
Email: zhen.gao@ntnu.no

ABSTRACT

A new numerical method, which is based on three-dimensional (3D) potential flow theory and finite element method (FEM), is used to predict the wave-induced hydroelastic responses of flexible floating bridges. The floating bridge is discretized into several modules based on the positions of the pontoons which are connected by elastic beams. The motion equations of the entire floating structure are established according to the six degrees of freedom (6DOF) motions of each rigid module coupled with the dynamics of the elastic beams. The hydrodynamics loads on each module are considered as external loads and simultaneously applied. The method is extended to take into account the shore side effect, which is obtained from the 3D potential flow theory and considered as a hydrodynamic boundary condition. The effects of inclination of shore side on the responses of the bending moment, horizontal and vertical displacements of the pontoon and their distribution along the bridge are investigated. The results show that the displacement response increase with an increasing steepness of the shore side.

Keywords: VLFS; Floating Bridge; Hydrodynamic Loads; Potential Flow Theory;

INTRODUCTION

The E39 main road at the west coast of Norway is planned to be upgraded by Norwegian Public Roads Administration (NPRA). The main goal is to replace the ferries for fjord-crossing by floating bridges. There are three main types of floating bridges or tunnels that were suggested, i.e. suspension bridge with floating tower supports, pontoon-supported surface bridge and floating tunnels [1]. Because of the large water depth (more than 500 meters), the surface crossing concept will greatly decrease the cost of this project, compared with the underwater floating tunnel concept. One of the concepts of floating bridge crossing Masfjorden was studied by Lie et al. [2], which is 700 meters long, with a water depth of 500 m.

A floating structure with a dimension of several hundred meters will become flexible, and is often labeled as *very large floating structure* (VLFS). It is different from traditional marine structures, since strong coupling between the structural deformations and fluid motions, which should be considered by hydroelasticity method. Frequency domain hydroelasticity theories have been developed from two-dimensional [3,4] to

*Corresponding Author: Shixiao Fu, E-mail: shixiao.fu@sjtu.edu.cn

three dimensional [5,6], from linear [7,8] to nonlinear models [9-11]. This concept has been used in many different purposes, such as floating airport and oil storage [12]. Floating bridge is one type of VLFS, in which the longitudinal dimension is much larger than either the transverse or the vertical dimension.

Hydroelasticity is an important design consideration for VLFS. The response of a VLFS in waves normally include two parts, i.e. rigid body motions (6DOFs) and structural deformations. Firstly, 6DOFs rigid body motions of floating structure in waves could be calculated through traditional sea keeping theory which is normally based on numerical methods using a panel model. In a traditional way, panel method based on potential flow theory and is used to calculate wave forces on the structures and finite element method (FEM) is used to predict deformations and stresses of the structures, respectively. In a hydroelastic analysis, external wave loads on the structure and its deformations are obtained simultaneously. In other words, in addition to the rigid-body motions, the effect of structural deformations on the hydrodynamic load distribution is also considered in such analysis. From the view of hydroelasticity, the deformation of the structures might be considered using a mode-superposition method. A new method for the hydroelastic responses of flexible floating structures in waves, which is so called "Discrete Modules Based" method has been recently proposed by Wei et al. [13] where, a VLFS will be divided into sub-modules connected by series elastic beams, and each sub-module is regarded as a rigid body. Under this circumstance, the motions of each module are affected by the hydrodynamic interactions with the surrounding modules and are restricted by the displacement continuity of adjacent modules. The displacement continuity between modules is guaranteed by the elastic beam system. The traditional methods based on the mode-superposition technique can be used for 'continuous' structures under wave loads, such as floating airport, floating tunnel, while this new method was developed for 'discrete' structures such as the MOB (Mobile Offshore Base) concept, pontoon-supported floating bridge, suspension bridge supported by floating towers.

Neglecting the hydrodynamic coupling effect between adjacent pontoons and the effect of the fjord boundary (shore sides), Lie et al. [2] investigated the hydroelasticity of two floating tunnel/bridge under waves and current. However, some researches indicated that the two neglected factors sometimes could have non-negligible influences on the hydrodynamics of each module [16].

In this paper, comparison among different cases are shown which with/without the hydrodynamic coupling, with/without the shore side effect. The basic theory of hydroelasticity on floating structure will be briefly discussed firstly. Following that hydrodynamic analysis of the pontoon is shown by taking the effect of hydrodynamic coupling (12 pontoons) and fjord boundary conditions (shore side) into account. Then the structural elements of the bridge and pontoons will be coupled together to show the hydrodynamic effect on the structural response. Distributions of the horizontal, vertical displacements and bending moment along the bridge in the conditions of accounting hydrodynamic coupling and fjord boundary conditions will be shown at last. From the analysis, we can see that the hydrodynamic coupling will decrease the response amplitude while the shore side effect can increase it at the same time. However, with a decreasing steepness of the shore side, the displacement response decreases.

BASIC THEORY

Hydrodynamic Analysis`

Three right-handed coordinate systems are introduced in the derivation of the wave-induced loads and responses, i.e. the global coordinate system *OXYZ*, body-fixed coordinate system $o_m x_m y_m z_m$ and reference coordinate system $o'_m x'_m y'_m z'_m$ ($m = 1, 2, ..., N$). The global coordinate system 'OXYZ' remains fixed in space, with 'OXY' at the still water surface and the 'Z' axis oriented straight up. The body fixed coordinate system $o_m x_m y_m z_m$ moves with the floating modules and is parallel to the coordinate axes of the global coordinate system *OXYZ* in its initial position. The reference coordinate system $o'_m x'_m y'_m z'_m$ coincides with the body-fixed coordinate system $o_m x_m y_m z_m$ in the initial stage and always remains at the balance position. The fluid around the floating structure is assumed to be ideal (i.e., inviscid, incompressible and irrotational). Hence the fluid behavior can be described by the velocity potential in global coordinate system as,

$$\Phi(X,Y,Z,t) = \phi(X,Y,Z)e^{-i\omega t} \qquad [1]$$

In which, ω is the circular wave frequency of incident wave and ϕ denotes the time-independent space complex.

For multi-module system, ϕ can be decomposed into:

$$\phi = \phi_I + \phi_D + \sum_{m=1}^{N} \phi_R^{(m)} \qquad [2]$$

In which, ϕ_I and ϕ_D represent the incident wave potential and diffraction potential, respectively. $\phi_R^{(m)}$ refers to the radiation potential of module *m*, which can be further expressed as,

$$\phi_R^{(m)} = -i\omega \sum_{j=1}^{6} \xi_j^m \phi_{jR}^{(m)} \qquad [3]$$

where the $\phi_{jR}^{(m)}$ shows the unit radiation velocity potential, in which the module *m* oscillates in a unit velocity in the *j*

direction with the other modules fixed, and ξ_j^m means the complex motion amplitude of the module 'm' in the *j-th* mode.

The incident wave potential at a finite water depth can be expressed as the following in the global coordinate system *OXYZ*.

$$\phi_I = \frac{igA}{\omega}\frac{\cosh\left[k\left(Z+H\right)\right]}{\cosh\left(kH\right)}e^{ik\left(X\cos\theta+Y\sin\theta\right)} \qquad [4]$$

where *A* and *H* denote the incident wave amplitude and water depth, respectively. *k* and θ mean the wave number and wave direction.

The radiation potential $\phi_{jR}^{(m)}$ of module *m* satisfies the Laplace equation in the fluid domain Ω, and boundary conditions including linearized free-surface condition (S_F), body surface conditions (S_n), sea bottom conditions (S_B), distant radiation condition (S_∞) and shore side condition (S_s). Since the body surface boundary conditions are consistent with the actual situation, solving this model in mathematics is reasonable.

$$\begin{cases} in\ \ \Omega:\nabla^2\phi_{jR}^{(m)}=0 \\ on\ \ S_F:-\omega^2\phi_{jR}^{(m)}+g\left.\dfrac{\partial\phi_{jR}^{(m)}}{\partial z}\right|_{z=0}=0 \\ on\ \ S_n:\dfrac{\partial\phi_{jR}^{(m)}}{\partial n^{(n)}}=\begin{cases} n_j^{(m)}, & m=n \\ 0, & m\neq n \end{cases} \\ on\ \ S_B:\left.\dfrac{\partial\phi_{jR}^{(m)}}{\partial n}\right|_{S_B}=0 \\ on\ \ S_\infty:\lim\limits_{r\to\infty}\left(r^{1/2}\left(\dfrac{\partial\phi_{jR}^{(m)}}{\partial r}-ik\phi_{jR}^{(m)}\right)\right)=0 \\ on\ \ S_S:\left.\dfrac{\partial\phi_{jR}^{(m)}}{\partial n}\right|_{S_S}=0 \end{cases} \qquad [5]$$

In the diffraction problem, all modules are fixed in the domain, with an incident wave acting on them. Similar to the radiation problem, the diffraction potential ϕ_D can be obtained from the governing equation and the boundary conditions in the fluid domain but with different body boundary condition,

$$on\ \ S_0:\frac{\partial\phi_D}{\partial n}=-\frac{\partial\phi_I}{\partial n},\qquad S_0=\sum_{m=1}^{N}S_m \qquad [6]$$

Firstly, the radiation and diffraction potential are calculated based on three-dimensional Green's function method. Then the dynamic fluid pressure which acts on the mean wetted surface can be obtained by the linearized Bernoulli equation. Finally, by integrating the pressure along the mean wetted surface, the *j-th* order wave excitation force of module *m* in the body-fixed coordinate system can be expressed as,

$$F_{wj}^{(m)}=\iint_{S_m}pn_j^{(m)}ds=i\rho\omega e^{-i\omega t}\iint_{S_m}\left(\phi_I+\phi_D\right)n_j^{(m)}ds \qquad [7]$$

This force including two parts:

$$\begin{cases} F_{Kj}^{(m)}=i\rho\omega e^{-i\omega t}\iint_{S_m}\phi_I n_j^{(m)}ds \\ F_{Dj}^{(m)}=i\rho\omega e^{-i\omega t}\iint_{S_m}\phi_D n_j^{(m)}ds \end{cases} \qquad [8]$$

where the first one is the Froude-Krylov force and the second one is the diffraction force.

The *j-th* order radiation force of body *m* generated by the free oscillations in the *k-th* mode of body *n* in body-fixed coordinate system can be expressed as:

$$F_{jk}^{(mn)}=\iint_{S_m}pn_j^{(m)}dS=\rho\omega^2\xi_k^{(n)}e^{-i\omega t}\iint_{S_m}\phi_k^{(n)}n_j^{(m)}dS \qquad [9]$$

Substituting the body boundary condition of radiation potential $\frac{\partial\phi_j^{(m)}}{\partial n}=n_j^{(m)}$ into the above formula,

$$A_{jk}^{(mn)}+\frac{iC_{jk}^{(mn)}}{\omega}=\rho\iint_{S_m}\phi_k^{(n)}\frac{\partial\phi_j^{(m)}}{\partial n}dS \qquad [10]$$

where the subscripts *k* and *j* represent the number of modes, while the superscripts *m* and *n* are the number of modules. $A_{jk}^{(mn)}$ and $C_{jk}^{(mn)}$ refer to the added mass and damping coefficients in the *j-th* mode of module *m* from the module *n* oscillating in the *k-th* mode, respectively.

Considering a floating system with N rigid modules, based on Newton's Second Law of Motion, the motion equation of the floating system in the reference coordinate system are expressed as:

$$\left(\begin{bmatrix} M^{(1)} & & \\ & \ddots & \\ & & M^{(N)} \end{bmatrix}+\begin{bmatrix} A^{(11)} & \cdots & A^{(1N)} \\ \vdots & \cdots & \vdots \\ A^{(N1)} & \cdots & A^{(NN)} \end{bmatrix}\right)\begin{Bmatrix} \ddot{x}^{(1)} \\ \vdots \\ \ddot{x}^{(N)} \end{Bmatrix}+\begin{bmatrix} C^{(11)} & \cdots & C^{(1N)} \\ \vdots & \cdots & \vdots \\ C^{(N1)} & \cdots & C^{(NN)} \end{bmatrix}\begin{Bmatrix} \dot{x}^{(1)} \\ \vdots \\ \dot{x}^{(N)} \end{Bmatrix}+\begin{bmatrix} K^{(1)} & & \\ & \ddots & \\ & & K^{(N)} \end{bmatrix}\begin{Bmatrix} x^{(1)} \\ \vdots \\ x^{(N)} \end{Bmatrix}=\begin{Bmatrix} F_w^{(1)} \\ \vdots \\ F_w^{(N)} \end{Bmatrix} \qquad [11]$$

where $\ddot{x}$, $\dot{x}$ and x are the rigid body acceleration array, velocity array and displacement array respectively, $\left[M^{(N)}\right]$ is the mass matrix of the *N-th* floating module; $\left[A^{(NN)}\right]$ and

$\left[C^{(NN)}\right]$ are added mass and damping matrices of module N. $\left[K^{(NN)}\right]$ refers to the hydrostatic restoring coefficient matrix. $\left\{F_w^N\right\}$ is the wave excitation force and moment, which can be easily obtained from Eq.7.

Structure Response Analysis

The continuous bridge used to connect adjacent modules has been assumed as Euler-Bernoulli beam. The structural stiffness matrix of elastic beams can be established based on structural mechanics and finite element methods.

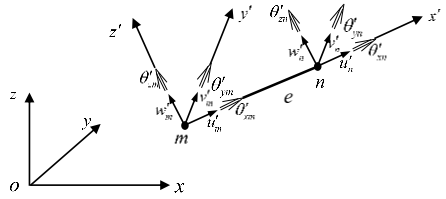

Figure 1 Two Coordinate Systems

In the structural analysis, two coordinate systems, namely, the local coordinate system ($mx'y'z'$) and global coordinate system ($OXYZ$) are used as Fig.1 shown. Stiffness matrix of each element in local coordinate system can be obtained based on Young's module and cross-sectional properties. The stiffness matrix in the local coordinate system can be transformed to the global coordinate system based on small deformation assumption,

$$\left[k\right]^e = \left[T^e\right]^T \left[k'\right]^e \left[T^e\right]$$

$$\left[\lambda\right] = \begin{bmatrix} \cos(x'x) & \cos(x'y) & \cos(x'z) \\ \cos(y'x) & \cos(y'y) & \cos(y'z) \\ \cos(z'x) & \cos(z'y) & \cos(z'z) \end{bmatrix} \quad [12]$$

Where $\left[T^e\right] = \begin{bmatrix} \lambda & & & \\ & \lambda & & \\ & & \lambda & \\ & & & \lambda \end{bmatrix}$ is the element variation matrix; $\left[k\right]^e$ is the element stiffness matrix of element *e* in the global coordinate system. Stiffness matrix of whole structure can be seen as summation of all element stiffness obtained above.

$$\left[k\right] = \begin{bmatrix} k_{11}^1 & k_{12}^1 & & & & \\ k_{21}^1 & k_{22}^1 + k_{22}^2 & k_{23}^2 & & & \\ & k_{32}^2 & k_{33}^2 + k_{33}^3 & & & \\ & & & \cdot & & \\ & & & & \cdot & \\ & & & & & k_{NN}^N \end{bmatrix} \quad [13]$$

In the structure analysis, structural damping is simplified using the Rayleigh damping model, so motion equation in the global coordinate system can be defined as:

$$\begin{aligned} &[m]\left\{\ddot{\delta}\right\} + \left[c\right]\left\{\dot{\delta}\right\} + \left[k\right]\left\{\delta\right\} = \left\{F\right\} \\ &\left[c\right] = \mu[m] + \lambda\left[k\right] \end{aligned} \quad [14]$$

where $\left\{F\right\}$ means the external loads in the global coordinate system, $\left\{\delta\right\}$, $\left\{\dot{\delta}\right\}$ and $\left\{\ddot{\delta}\right\}$ are the displacement, velocity and acceleration vectors, respectively. $\left[k\right]$ is the stiffness matrix of the whole structure in Eq.13. $[m]$ and $\left[c\right]$ refer to the mass matrix of the bridge only and structural damping matrix, respectively. 'μ' and 'λ' are constant number.

Coupled Equation of Motions and Structural Deformations in Frequency Domain

Responses of the floating bridge consist of rigid body's motion responses of the pontoons and the structure's elastic deformation responses of the bridge. Since every beam section connecting adjacent pontoons could be divided into several elements, we assumed the number of beam element is *q*. Then the global stiffness matrix has dimension $6L \times 6L, L = q+1$ *L* is also the number of nodes for beam system. Combining the hydrodynamic parameters and the structural deformation, Eq.15 can be got, where $[m]$ is the mass matrix of the beam system, $\left[k_{LL}^L\right]$ denotes the structural stiffness sub-matrix of the element of the connecting beam. $\left[\delta^{(L)}\right]$ is the displacement array of the node *L* of the beam and part of them when the beam node *L* at the same potion of body *N*, it is also the displacement array of body *N*. $\left[F^{(L)}\right]$ is the external force array, which includes hydrostatic restoring force $\left[K\right]\left\{\delta\right\}$, inertial force $\left[M\right]\left\{\ddot{\delta}\right\}$. wave excitation force $\left\{F_w\right\}$ and wave radiation force, which contains two components: the added mass force $\left[A\right]\left\{\ddot{\delta}\right\}$ and potential damping force $\left[C\right]\left\{\dot{\delta}\right\}$.

$$\begin{bmatrix} m^{(1)} & & & & \\ & m^{(2)} & & & \\ & & m^{(3)} & & \\ & & & \ddots & \\ & & & & m^{(L)} \end{bmatrix} \begin{Bmatrix} \ddot{\delta}^{(1)} \\ \ddot{\delta}^{(2)} \\ \ddot{\delta}^{(3)} \\ \vdots \\ \ddot{\delta}^{(L)} \end{Bmatrix} + \left\{ \mu \begin{bmatrix} m^{(1)} & & & & \\ & m^{(2)} & & & \\ & & m^{(3)} & & \\ & & & \ddots & \\ & & & & m^{(L)} \end{bmatrix} + \lambda \begin{bmatrix} k_{11}^1 & k_{12}^1 & & & \\ k_{21}^1 & k_{22}^1+k_{22}^2 & k_{23}^2 & & \\ & k_{32}^2 & k_{33}^2+k_{33}^3 & \ddots & \\ & & & \ddots & k_{LL}^L \end{bmatrix} \right\} \begin{Bmatrix} \dot{\delta}^{(1)} \\ \dot{\delta}^{(2)} \\ \dot{\delta}^{(3)} \\ \vdots \\ \dot{\delta}^{(L)} \end{Bmatrix} + \begin{bmatrix} k_{11}^1 & k_{12}^1 & & & \\ k_{21}^1 & k_{22}^1+k_{22}^2 & k_{23}^2 & & \\ & k_{32}^2 & k_{33}^2+k_{33}^3 & \ddots & \\ & & & \ddots & k_{LL}^L \end{bmatrix} \begin{Bmatrix} \delta^{(1)} \\ \delta^{(2)} \\ \delta^{(3)} \\ \vdots \\ \delta^{(L)} \end{Bmatrix} = \begin{Bmatrix} F^{(1)} \\ F^{(2)} \\ F^{(3)} \\ \vdots \\ F^{(L)} \end{Bmatrix} \quad [15]$$

In the Eq.15, m denotes the mass of the beam girder, displacement and wave excitation force are the function of the time and space, which make periodic variation with stable frequency, they can be rewritten as $\{\delta\} = \{x\} e^{-i\omega t}, \{F_w\} = \{f_w\} e^{-i\omega t}$,

where, x and f_w denote the complex amplitudes of the displacement and wave excitation force vectors, respectively.

Consequently, Eq.15 can be written as,

$$\begin{pmatrix} -\omega^2\left([M]_{6L\times 6L} + [A]_{6L\times 6L} + [m]_{6L\times 6L}\right) - i\omega\left(\mu[m]_{6L\times 6L} + \lambda[k]_{6L\times 6L}\right) \\ -i\omega[C]_{6L\times 6L} + [K]_{6L\times 6L} + [k]_{6L\times 6L} \end{pmatrix} \{x\}_{6L\times 1} = \{f_w\}_{6L\times 1} \quad [16]$$

Based on above discussion, structure displacement can be got as complex numbers and their amplitudes can be used to obtain the structure response under the corresponding wave frequency ω.

Coupled Equation of Rigid-body Motion and Flexible-body Deformation in Time Domain (SIMA)

The time domain hydrodynamic analysis theory has been established by Cummins (1964) based on the linear assumption and impulse response function. For the multi-module system connected by elastic beams, this time domain motion equation in the global coordinate system can be expressed as,

$$\left[M+m+A(\infty)\right]_{6L\times 6L}\left\{\ddot{\delta}(t)\right\}_{6L\times 1} + [c]_{6L\times 6L}\left\{\dot{\delta}(t)\right\}_{6L\times 1} + [K+k]_{6L\times 6L}\left\{\delta(t)\right\}_{6L\times 1} + \int_{-\infty}^{t}\left[H(t-\tau)\right]_{6L\times 6L}\left\{\dot{\delta}(\tau)\right\}_{6L\times 1} d\tau = \left\{F_w(t)\right\}_{6L\times 1} \quad [17]$$

In which, $A(\infty)$ is the added mass matrix in the infinite wave frequency; $\left[H(t)\right]$ is the retardation function matrix; and its integral $\int_{-\infty}^{t}\left[H(t-\tau)\right]\left\{\dot{\delta}(\tau)\right\} d\tau$ represents the fluid memory effect; $\left\{F_w(t)\right\}$ is the first order wave excitation force in time domain. Other terms have the same meanings as the forgoing descriptions.

The retardation function can be expressed by the frequency result of added mass or damping coefficients, based on Kramer-Kronig relations, which relies on Fourier transform by Ogilvie (1964).

$$\begin{aligned} \left[H(t)\right] &= -\frac{2}{\pi}\int_0^{\infty} \omega\left[A(\omega) - A(\infty)\right]\sin(\omega t)\, d\omega \\ &= \frac{2}{\pi}\int_0^{\infty}\left[C(\omega)\right]\cos(\omega t)\, d\omega \end{aligned} \quad [18]$$

where $A(\omega)$ and $C(\omega)$ denote the added mass and damping coefficients in the frequency domain, respectively.

When the motion equation induced, the static analysis of whole structure will be done firstly, from which the static deformation, pre-stress of the system by static buoyancy force on the pontoons, self-weights of the beams will be acquired. The calculated static response including, deformation and pre-stress will be treated as initial condition of the whole bridge in dynamic analysis. The dynamic simulation based on step by step numerical integration of the dynamic equilibrium equations, response of the floating structure can be obtained. The integration method used here is based the well-known Newmark β family including the Wilson θ method considering a constant time step. Wave force and hydrodynamic coefficients of all pontoons are obtained from WAMIT, while a time domain code, SIMA is used to solve the equations of motions considering the bridge as flexible beams. Time-domain analysis with series regular incident waves was performed using SIMA.

FLOATING BRIDGE

The concept of a floating bridge supported by discrete pontoons has been proposed in Norway. Overall bridge model is shown in Fig.2, which has been proposed by Lie et al., [2]. All pontoons and connecting girders have been numbered as P1, B0 to P12, B12 from the left side to right, respectively. This bridge consists of:

1) Two continuous bridge sections of about 350m each, simply connected with each side of the fjord.
2) 10 large pontoons supporting the bridge section. (P1-P5, P8-P12)
3) One 72 m bridge section hinged to one of the long bridge sections.
4) 2 smaller pontoons supporting the swing lane (P6 and P7)

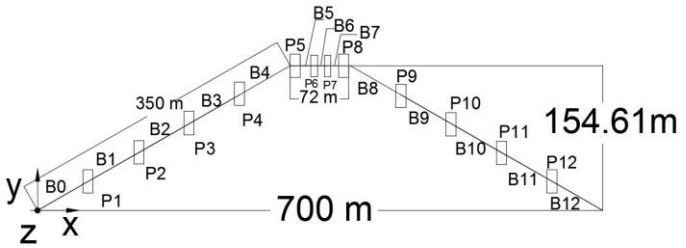

Figure 2 Arrangement of the Pontoon Supported Girder Concept

Fig.2 shows the top view of the floating bridge, which is simply connected to the shore sides at both left and right ends. Main parameters of each pontoon are shown in Tab. 1.

Table 1 Dimensions of the Pontoons

Pontoon No.	**Length (m)**	**Breadth (m)**	**Draught (m)**	**Submerged Volume (m^3)**
P1-P4, P9-P12	28	12	4.98	1519.38
P5, P8	28	12	2.27	692.57
P6, P7	26	8	4.43	860.60

The detail information of the upper bridge girder and road are listed in Tab 2.

Table 2 Cross Section Data for Bridge Girder

Mass per Length	m	1.6e+04	kg/m
Axial Stiffness	EA	1.025e+11	N
Bending Stiffness Y	EI(y)	6.882e+10	Nm^2
Bending Stiffness Z	EI(z)	9.030e+11	Nm^2

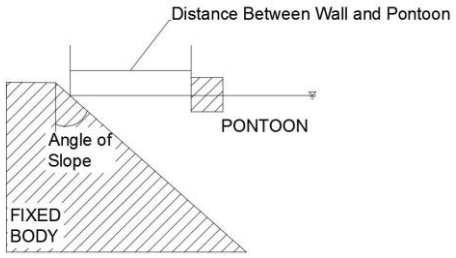

Figure 3 Illustration of the Pontoon Close to the Fjord Shore Side

The effects of the sloped angles of the shore (0, 30, 45) as defined in Fig.2, have been investigated in this paper. Moreover, positions of all 12 pontoons in global coordinate system are listed in Tab.3.

Table 3 Position of Each Pontoon in the Global Coordinate System

Pontoon No.	**X Coordinate (m)**	**Y Coordinate (m)**	**Z Coordinate (m)**
P1	62.8	30.922	0
P2	125.6	61.844	0
P3	188.4	92.766	0
P4	251.2	123.688	0
P5	314	154.61	0
P6	338	154.61	0
P7	362	154.61	0
P8	386	154.61	0
P9	448.8	123.688	0
P10	511.6	92.766	0
P11	574.4	61.844	0
P12	637.2	30.922	0

NUMERICAL MODELS

Hydrodynamic coefficients of all pontoons in different cases are calculated through potential theory software WAMIT [23]. The bridge girders are modeled by beam finite elements in the time-domain simulation tool SIMA [22].

Hydrodynamic Model

In this study, pontoons and shore sides have all been modelled through the panel method. Each pontoon is simplified as rigid floating body with 6 DOFs. The hydrodynamic coefficients (added mass and potential damping coefficients) are directly calculated by the panel model in WAMIT. The panel models of the floating pontoons are illustrated in Fig.4.

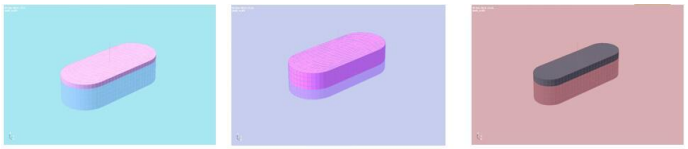

Figure 4 Hydrodynamic Mesh of the Three Kinds of Floating Pontoons

Hydrodynamic interaction between adjacent pontoons has been considered in this study as Fig.5 shows, with three colors present three different types. Since the up limitation of the panel number, the mesh size of the pontoons cannot be as small as one tenth of the incident wave length as usual. Therefore, sensitivity study of the mesh size will be shown in the section of 'Verification of Numerical Models'.

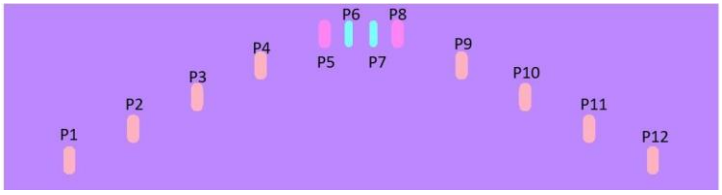

Figure 5 Hydrodynamic Model Considering the Interaction between the Pontoons

Sloped shore sides restrict the water area in this study. To describe the character of different shores, ‘sloped angle’ and ‘distance from shore side to pontoon’ have been defined in the Fig.3.

Fig.6 shows the three different sloped shores considered in this study.

Figure 6 Hydrodynamic Mesh of Different Shores

All the three shore sides are 1000m long and 520m high. To obtain hydrodynamic effect, two shore sides and twelve pontoons are considered together as Fig.7 shown.

Figure 7 Panel Model for Shore Side Effects

In the hydrodynamic study of pontoons, three typical cases have been considered.

1. Single pontoon in open sea
2. Multi-pontoons in open sea
3. Multi-pontoons in the sea restricted by shore sides

Structural Model

The girder and main road are structurally modeled as slender beams by 12-DOF beam elements with 2 symmetry planes to deal with the different stiffness properties in horizontal and vertical directions as Fig.8 shows.

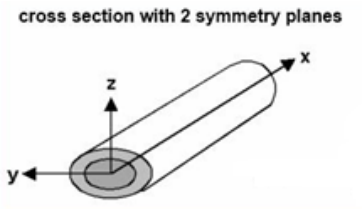

Figure 8 Beam Element with Two Symmetry Planes [20-21]

All pontoons are connected by the elastic beam element.

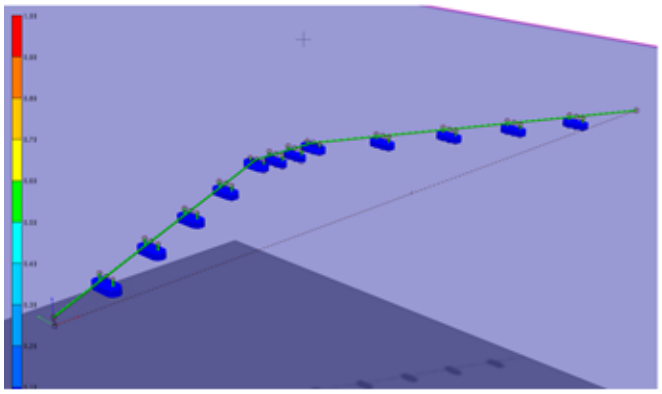

Figure 9 Numerical Model for Pontoon Supported Floating Bridge in SIMA

The dynamic system is integrated and coupled together by SIMA into finite element model by means of RIFLEX. Fig.9 shows the finite element model of the whole structure. Both of the left and right ends of the bridge are simply connected to the shore side, which refers to fixing all translations and free all rotations in the numerical model.

VERIFICATION OF NUMERICAL MODEL

Shore sides in fjord were represented by a fixed large body, which had been shown not easy to obtain reasonable result by Ferreira et al. [15]. Because serious transverse waves which are reflected back and forth between vertical sides, the result has to be verified.

Mesh Size Convergence Study

Fig.10 shows a convergence study on mesh size of a single pontoon, by comparing the added mass coefficients in heave. Obviously, there is almost no difference when the mesh size smaller than 2.5m. To carry out the following simulations successfully, the mesh size of each pontoon has been set as 2m.

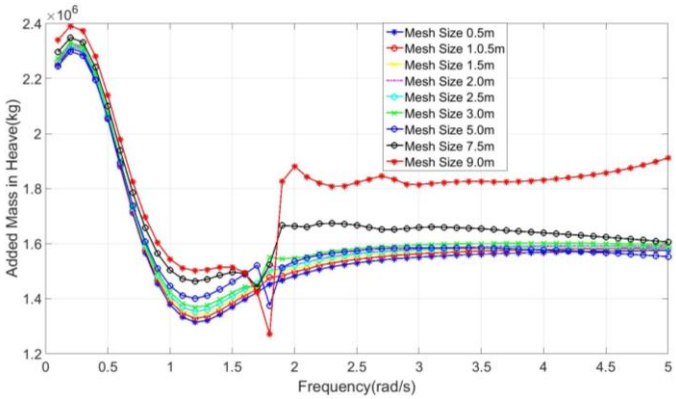

Figure 10 Sensitivity Study of Mesh Size

Difference Between Fixed Body and Infinitely-long Wall

From the result given by Korsmeyer et al. [16], it is not easy to get reasonable simulation when the shore is represented by a fixed body. Because serious transverse waves which are reflected back and forth between vertical sides. To ensure the accuracy, a default wall model with infinite length in WAMIT has been used here. In the default wall model, the wall is infinite long without thickness, which means no transverse wave generated. However, for the case of fixed body representing the shore, this has to be tested since the finite length of it.

The added mass and damping in heave and wave excitation force on the single pontoon in the two cases are compared to validate the accuracy of the 'fixed body'.

Fig.11 and Fig.12 show the result of the added mass and damping, in which, there is almost no difference.

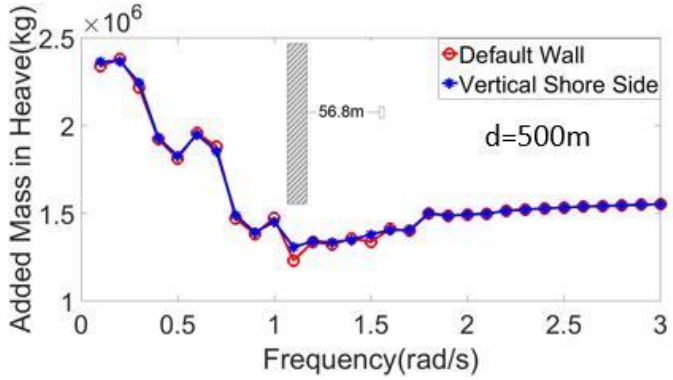

Figure 11 Comparison of Added Mass Between Default Wall Case and Vertical Shore Side Case

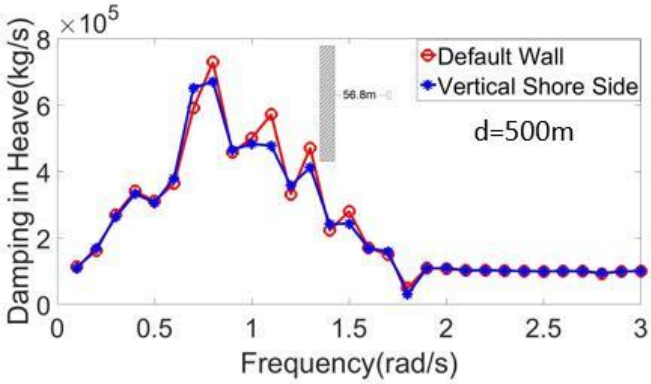

Figure 12 Comparison of Hydrodynamic Damping Between Default Wall Case and Vertical Shore Side Case

Fig.13 gives the frequency domain wave excitation force in these two cases. It is clearly seen, that the 'fixed body' is similar as the default wall, especially for frequency larger than 0.3 rad/s. Therefore, the fixed body can be used to replace the shore side in the following.

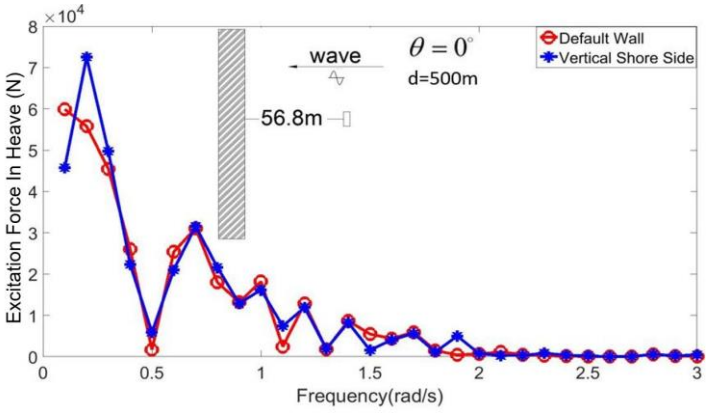

Figure 13 Comparison of Wave Exciting Force Between Default Wall Case and Vertical Shore Side Case

Comparison of the Time-domain and Frequency-domain Results

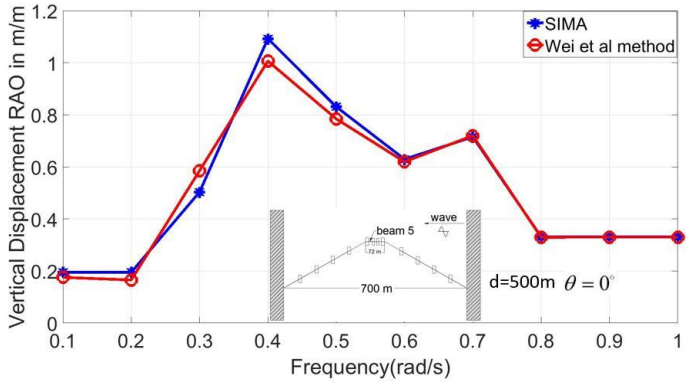

Figure 14 Comparison of the Heave RAO between SIMA and Wei's frequency-domain Code (Wei et al., 2017)

Wei et al. [13]'s frequency domain hydroelastic analysis code has been used in this study. Series unit amplitude regular waves flow from right to left in infinite water depth have been investigated here. The Wei's code has been verified through the comparison study with the existing result [8].

Response analysis of the whole structure has been done through SIMA and the Wei's code. Vertical displacement of the left end of the Beam5 is taken as an example shown in Fig.14. It is clearly seen, that the SIMA result agrees with the Wei's code result perfectly, especially for frequency larger than 0.6 rad/s.

RESULTS AND DISCUSSION

Modal Analysis of the Structure

Tab.4 shows the natural frequency of the first 10 modes in air. It can be noted that the natural frequency is very large, which

means the corresponding natural period is considerable small. The wave period is normally larger than the natural period of the structure. Because the wave length in fjord is normally larger than 100m (Lie et al. (2016)).

Table 4, Natural Frequency of the Structure

Mode	Fre. (rad/s)	Mode	Fre. (rad/s)
1	0.723	6	5.646
2	1.162	7	6.269
3	2.592	8	6.645
4	3.648	9	9.265
5	5.494	10	9.556

Fig. 15 shows the shape of the first and second mode. There is no vertical displacement for 1st mode and no horizontal displacement for second mode. To discuss the hydrodynamic coupling and shore side effect, series of regular incident waves with small frequencies were used in this study.

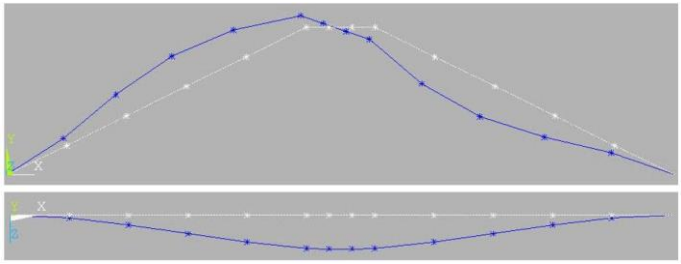

Figure 15 Shape of 1st and 2nd Mode

Results of the structure response for the two typical cases, in which the specific effect is considered, will be discussed in this part,

- Hydrodynamic coupling effect.
- Shore side effect.

Hydrodynamic Coupling Effect

The pontoon P6 is chosen to study the hydrodynamic coupling effect since the distance from it to adjacent modules is in the same order of its dimensions. Comparative study of hydrodynamic coefficients and wave excitation force for P1 and P5 are also shown in the appendix. The hydrodynamic coupling effect on P1 can be neglected since the large distance to the adjacent modules.

Fig.16 shows the comparison study of added mass of P6. Admittedly, adjacent pontoons induce many wiggles in the case of the small frequency. While, their effects can be neglected when the frequency is larger than 1.7 rad/s. Consider the mutual impact among pontoons, the added mass is a little larger when the hydrodynamic coupling is taken into account, which might decrease response amplitude.

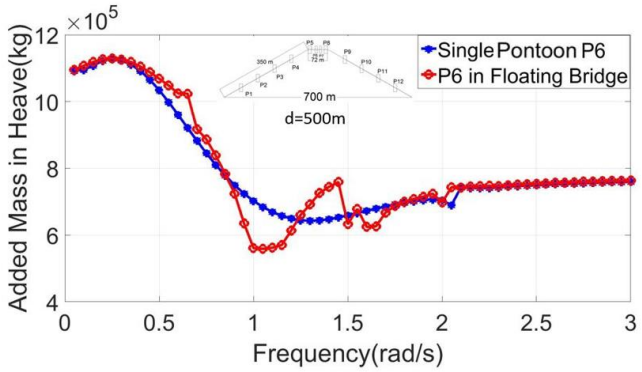

Figure 16 Added Mass for Single and Multi-Body Cases

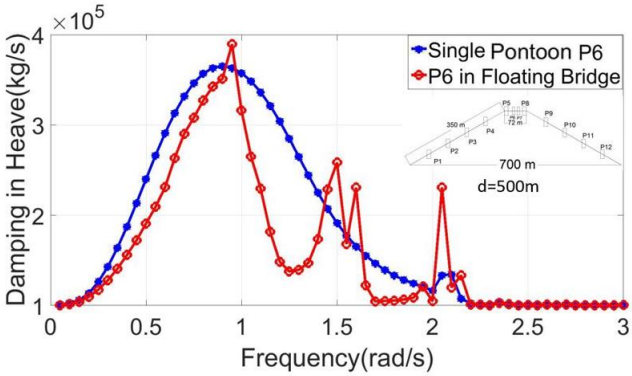

Figure 17 Hydrodynamic Damping for Single and Multi-Body Cases

Fig.17 shows hydrodynamic coupling effect on the damping of P6. The first peak of the two lines appear at almost same frequency around 0.7 rad/s. Then a larger peak appears in the 'multi-module' line corresponding to frequency around 0.9 rad/s. When the frequency larger than the 2.1 rad/s, there is almost no difference between them. When the floating structure is oscillating, the waves are radiating to the surrounding area. The energy taken away by waves should be provided by the floating structure, the kinetic energy of structure is mainly consumed by energy diffusion, while the existence of adjacent floating structures has obstructed energy diffusion during the movement of free floating structure, which reduces the energy consumption at the same time and it equals to the decline of damping value.

Fig.18 shows the comparison result for the wave excitation force with series of regular waves coming from 'west'. Shielding effects from adjacent pontoons lead smaller incident wave amplitude for P6. Therefore, the wave excitation force in the single pontoon condition is a little larger than it in multi-pontoons condition.

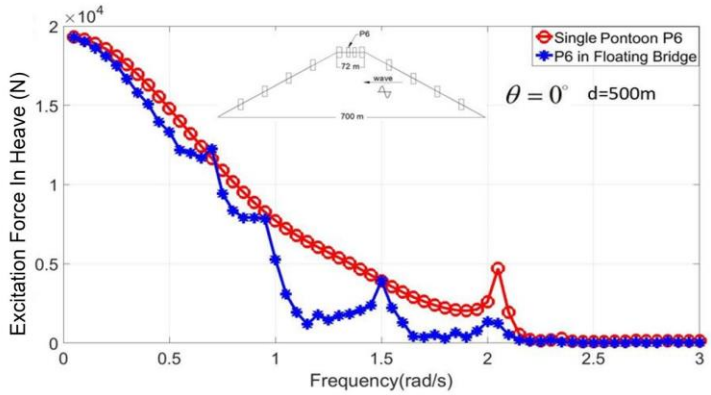

Figure 18 Wave Exciting Force in Heave for Single and Multi-Body Cases

Fig.19 and Fig.20 shows the comparison result of horizontal and vertical displacement. Since the incident wave coming from 'north-west' direction, the left part of the bridge experiences a little larger displacement.

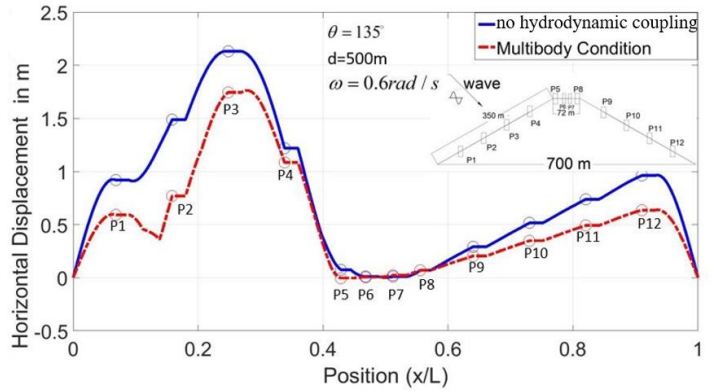

Figure 19 Horizontal Displacement for Single and Multi-Body Cases

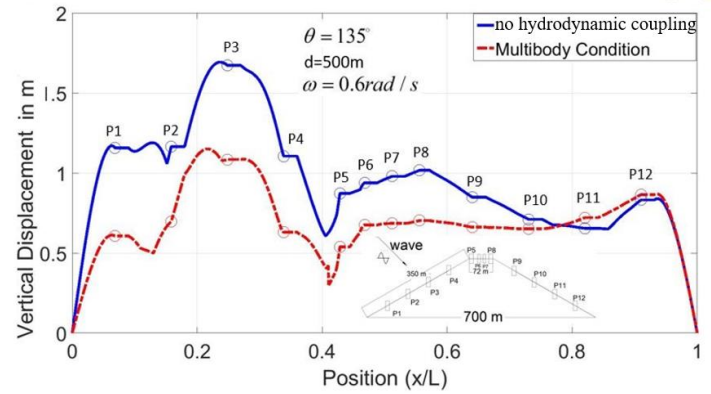

Figure 20 Vertical Displacement for Single and Multi-Body Cases

Fig.21 shows the comparison result of bending moment along the floating bridge. There is small difference for these two cases in the right part (x/L>0.5). And larger bending moment could be induced by single pontoon's assumption for the left part. There are twelve peaks evenly arranged along the bridge corresponding to the middle of each beam which connecting discrete pontoons.

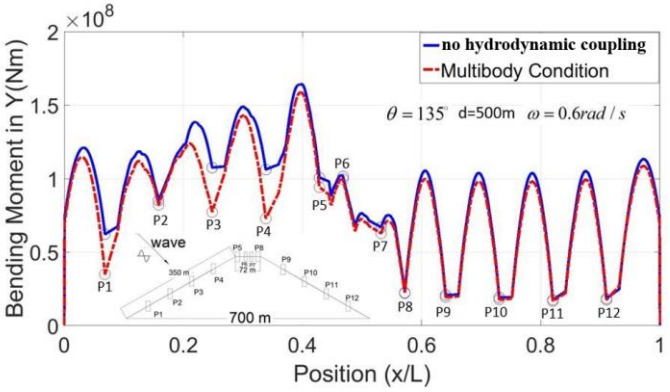

Figure 21 Vertical Bending Moment along the Bridge Girder for Two Conditions

Beam5 which connecting P5 and P6 is taken as an example to show the response amplitude with different incident wave frequency because the length of the beam has the same order with the dimensions of the pontoons. Incident wave was also assumed coming from 'north-west' in this case.

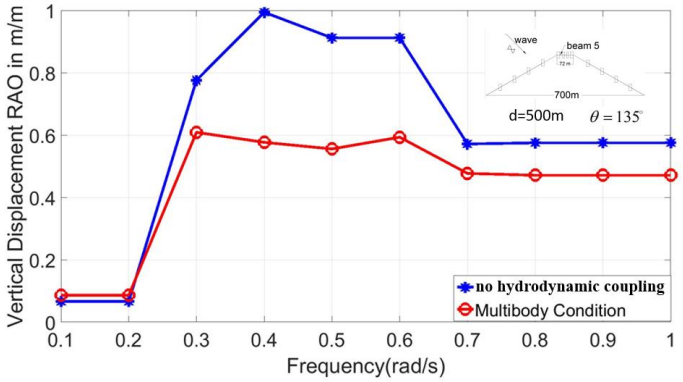

Figure 22 Vertical Displacement RAO of Left Point on B5

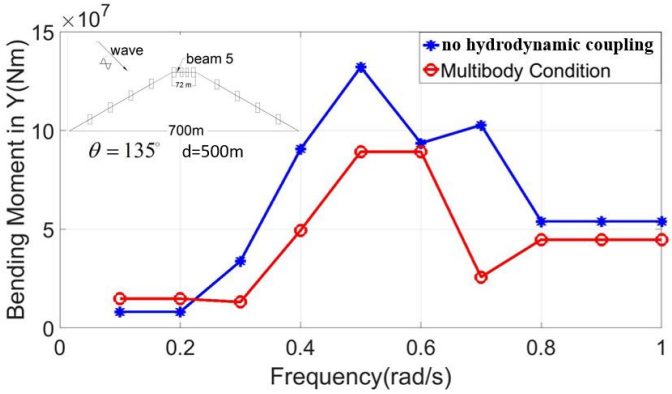

Figure 23 Vertical Bending Moment RAO of Left Point on B5

Fig.22 and Fig.23 shows the RAO of vertical displacement and bending moment. Generally speaking, all of them tend to stable when the incident wave frequency larger than 0.8 rad/s and the values in single pontoon condition are larger than them in multi-module condition. Vertical displacement in these two conditions share an almost same value in the low frequency part, which means the large incident wave length eliminate the hydrodynamic coupling effect. The difference of bending moment in low frequency part is also small. However, the dichotomy of them in large frequency part is also very small, so there is a range of frequency, in which the hydrodynamic coupling effect have to be carefully considered. Vertical displacement and bending moment of single pontoon condition could be 1.5-2 times of it in multibody condition within this range.

Effects from Adjacent Pontoon and Sloped Shore Sides

Three different shore models have been considered in this study with different sloped angles. Added mass, damping and wave excitation force for P1 will be used to show their effects.

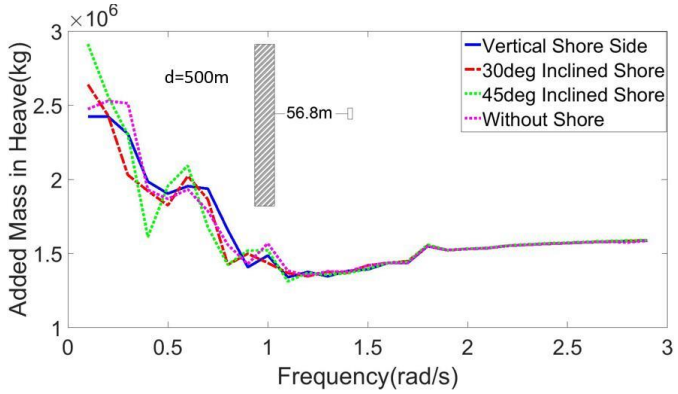

Figure 24 Added Mass for Different Sloped Shore Conditions

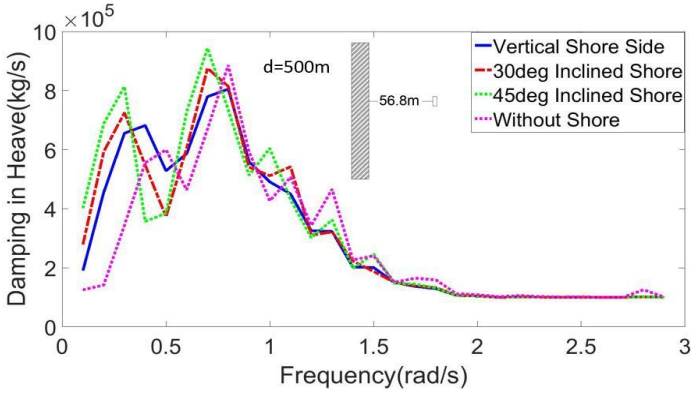

Figure 25 Hydrodynamic Damping for Different Sloped Shore Conditions

In this part, three different shore sides have been considered with sloped angle 0, 30 and 45. Fig.24 and Fig.25 shows the added mass and damping in three conditions are different from each other at the low frequency part, while the values become similar when the frequency larger than 1 rad/s. Moreover, the values in 45deg sloped shore condition is a little larger than the values in other two conditions. Through comparison with the case neglecting the shore side effect, added mass and damping are not affected a lot.

Different from added mass and damping, wave excitation force increases a lot when the slope angle decreasing as Fig.26 shown. The reason for this phenomenon is that the stronger wave reflection ability of the vertical shore side leads larger incident wave amplitude. Fig.26 also shows that wave excitation force in the condition without shore side is much smaller.

Sloped shore side's effect decreases a lot in the case of the distance to the shore side is large. Wave excitation force of P2 is shown in the appendix, the shore side effect is not as obvious as P1.

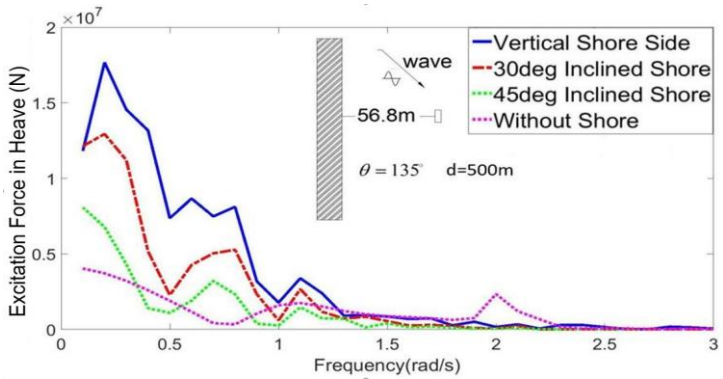

Figure 26 Wave Exciting Force in Heave for Different Sloped Shore Conditions

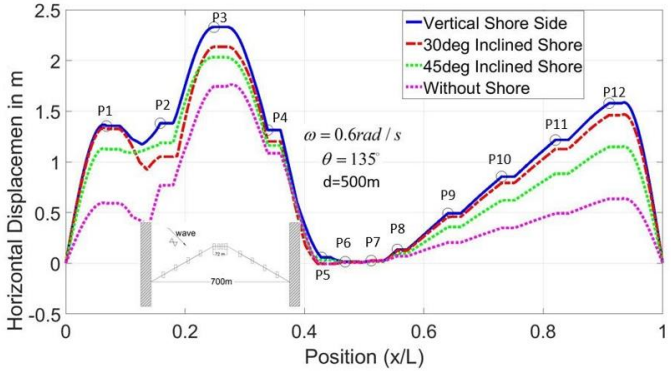

Figure 27 Horizontal Displacement for Different Sloped Shore Conditions

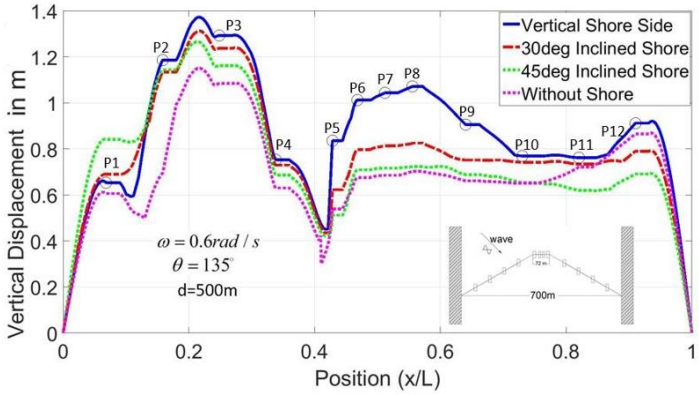

Figure 28 Vertical Displacement for Different Sloped Shore Conditions

Fig.27 and Fig.28 show the RAO of horizontal and vertical displacements along the bridge. Displacement of the middle part is smaller than the end parts due to the various distances to the shore side. Moreover, the vertical shore side leads much larger displacement due to its larger wave reflection ability.

Results for the condition without shore side have also been shown in the above figures. Its value is much smaller than others especially for the peak value, since there are no reflection waves.

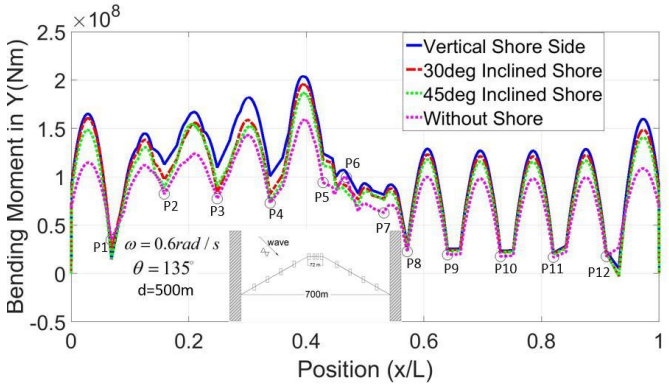

Figure 29 Vertical Bending Moment along the Bridge Girder for Different Sloped Shore Conditions

Fig.29 shows the comparison result of bending moment. Values of the condition with vertical shore side are much larger. Black circles in this figure show the positions of twelve pontoons along the bridge, it is clearly seen that most of them are at the valleys.

RAO of vertical displacement and bending moment of left point in B5 are shown in Fig.30 and Fig.31. Vertical shore side leads larger value of them in most frequency range. The difference between vertical shore side condition and other conditions is eliminated when the incident wave frequency smaller than 0.3 rad/s.

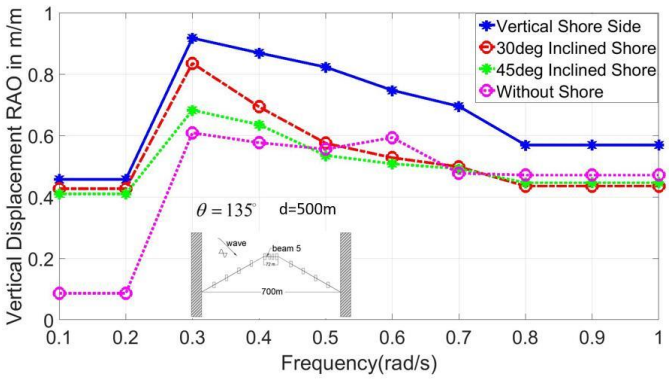

Figure 30 Vertical Displacement RAO of Left Point on B5

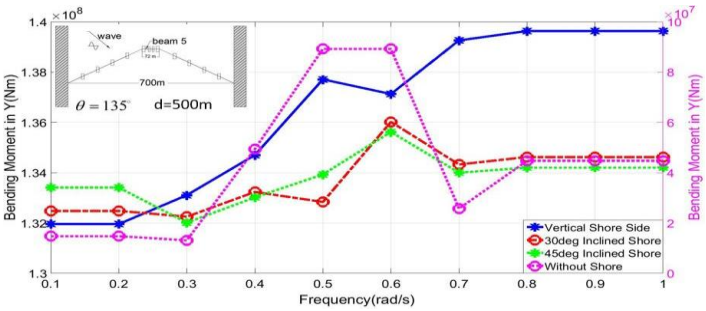

Figure 31 Vertical Bending Moment RAO of Left Point on B5 (line for without shore side corresponding to right axis)

CONCLUSION

Frequency domain analysis of floating bridge has been conducted in this study accounting for two effects, i.e. hydrodynamic coupling and fjord boundary condition (slope shore side). Fixed body is used to represent the shore side in hydrodynamic analysis.

For the case of accounting hydrodynamic coupling effects, added mass is larger in multibody condition, while the damping and wave excitation force are smaller. However, the values of them will be the same as the values for single pontoon in the case of large incident wave frequency. Response of the floating bridge in the case accounting hydrodynamic coupling is a little smaller than it in the case neglecting the coupling.

For the second case, sloped shore sides have limited effect on added mass and damping, while the wave excitation force is largely amplified. Floating bridge near shore side has larger response than it in the open sea, while the response amplitude of the structure could be decreased with the increasing of sloped angle.

REFERENCES

[1] A Feasibility Study- How to Cross the Wind and Deep Sognefjord, 2011, NPRA Report.
[2] Lie H., Fu S, Fylling I., Fredriksen A. G., Bonnemaire B., and Kjersem G. L.: "Numerical Modelling of Floating and Submerged Bridges Subjected to Wave, Current and Wind", Proc., Paper No. OMAE2016-54851, OMAE 2016 Conference, Busan, South Korea, pp. V007T006A075-V007T006A075.
[3] Betts, Bishop, R., & Price, W., 1977. The symmetric generalized fluid forces applied to a ship in a seaway. RINA Supplementary Papers, 119.
[4] Bishop, R., Price, W., & Temarel, P., 1979. A unified dynamical analysis of antisymmetric ship response to waves.
[5] Wu, Y., 1984. Hydroelasticity of floating bodies. University of Brunel.
[6] Chen, X., Moan, T., Fu, S., & Cui, W., 2005. Hydroelastic analysis of flexible floating structures in regular waves. Paper presented at the Proceedings of the International Conference on Mechanical Engineering and Mechanics, ICMEM.
[7] Wu, Y., Wang, D., Riggs, H. R., & Ertekin, R. C., 1993. Composite singularity distribution method with application to hydroelasticity. Marine Structures, 6(2-3), 143-163
[8] Fu S., Moan T., Chen X., and Cui W. (2007), 'Hydroelastic Analysis of Flexible Floating Interconnected Structures', Ocean Engineering 34 (11), 1516-1531.
[9] Chen, X., Wu, Y., Cui, W., & Tang, X., 2003. Nonlinear hydroelastic analysis of a moored floating body. Ocean Engineering, 30(8), 965-1003.
[10] Chen, X., Moan, T., Fu, S., & Cui, W., 2006. Second order hydroelastic analysis of a floating plate in multidirectional irregular waves. International Journal of Non-Linear Mechanics, 41(10), 1206-1218.
[11] Chen, X., Moan, T., & Fu, S., 2010. Extreme response of Very Large Floating Structure considering second-order hydroelastic effects in multidirectional irregular waves. Journal of Offshore Mechanics and Arctic Engineering, 132(4), 041601
[12] Wang C. M. and Tay Z. Y. (2011) 'Very Large Floating Structures: Applications, Research and Development', Procedia Engineering, Voll14, pp62-72.
[13] Wei, W., Fu, S., Moan, T., Lu, Z., & Deng, S. (2017), A discrete-modules-based frequency domain hydro-elasticity method for floating structures in inhomogeneous sea conditions. Journal of Fluids and Structures, 74, 321-339.
[14] Faltinsen O. M. (1993) Sea Loads on Ships and Offshore structures. *Cambridge University Press*.
[15] Ferreira M. D., Newman J. N., "Diffraction Effects and Ship Motions on an Artificial Seabed". *IWWWFB 2009 Workshop*, Zelenogorsk, Russia.
[16] Korsmeyer F. T., Lee C. H., and Newman J. N. (1993) Computation of Ship Interaction Forces in Restricted Waters. *Journal of Ship Research* 37 (04), 298-306.
[17] Mei C. C., Stiassine. M. and Yue D. K. P. (2005), 'Theory and Application of Ocean Surface Waves: Nonlinear Aspects (Vol.23), World Scientific.
[18] Newman J. N. (1977) Marine hydrodynamics. MIT press
[19] Ogilvie, T. F., 1964. Recent progress toward the understanding and prediction of ship motions. Paper presented at the 5th Symposium on naval hydrodynamics
[20] RIFLEX Theory Manual, 1995, Marintek Report.
[21] SIMO Theory Manual, 2001, Marintek Report.
[22] SIMA User Manual, 2014, Marintek Report.
[23] WAMIT User Manual, 2006, WAMIT

NOMENCLATURE

EI(y): Bending Stiffness about Y Axis
EI(z): Bending Stiffness about Z Axis
k: Wave Number ($\frac{2\pi}{\lambda}$)
r/dis: Distance from Pontoon to Shore
d: Water Depth
m: Mass of Beam Connecting Pontoons
$A_{kj}^{(mn)}$: Added Mass Coefficient
$C_{kj}^{(mn)}$: Damping Coefficient
λ : Wave Length
ϕ_I : Incident Potential
ϕ_D : Diffraction Potential
ϕ_R : Radiation Potential
A: Wave Amplitude
θ : Wave Direction

APPENDIX

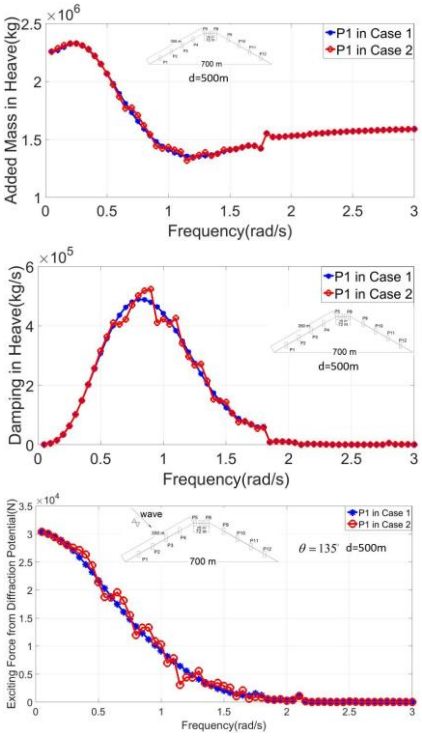

Added Mass, Damping and Wave Exciting Force for P1 in Case 1 and Case 2

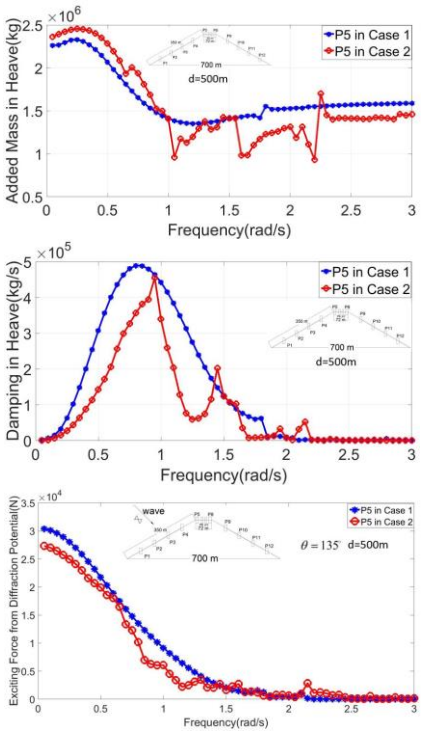

Added Mass, Damping and Wave Exciting Force for P5 in Case 1 and Case 2

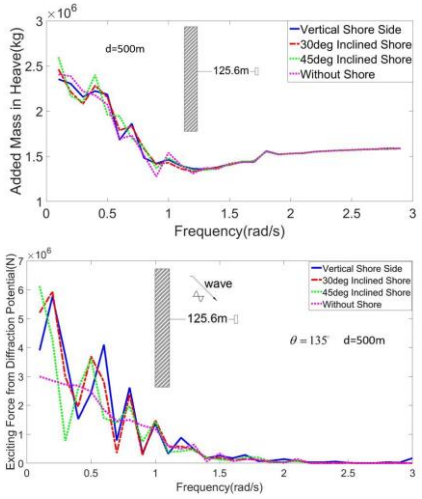

Added Mass and Wave Exciting Force for P2 in Case 3